

EARLY STAGE EXPERIMENT
Science Description

Experiment/Module: Analysis of Intensity Change Processes Experiment (AIPEX)

Investigator(s): Rob Rogers, Ghassan Alaka, Trey Alvey, Joe Cione, Jason Dunion, Michael Fischer, Heather Holbach, Paul Reasor, Jun Zhang, Josh Alland (NHC), Xiaomin Chen (Univ. Alabama Huntsville), Falko Judt (NCAR), Rosimar Rios-Berrios (NCAR), Josh Wadler (ERAU)

ONR TCRI Investigator(s): James Doyle (NRL), Dan Stern (NRL), Pete Finnochio (NRL), Sharan Majumdar (Univ. of Miami/RSMAS), David Nolan (Univ. of Miami/RSMAS), Tony Wimmers (Univ. of Wisconsin/CIMSS), Zeljka Fuchs (New Mexico Tech), David Raymond (New Mexico Tech), Brian Tang (SUNY Albany), George Bryan (NCAR), Michael Bell (CSU), and Ralph Foster (Univ. of Washington)

Requirements: TD, TS, Category 1

Plain Language Description: Predicting the timing and rate of tropical cyclone (TC) strengthening events remains one of the most challenging aspects of hurricane forecasting. In their early stages, the structure of developing storms is often disorganized such that their circulations are tilted in the vertical, have prominent dry air masses that can be transported into the inner circulation, and lack rainfall coverage all around the center. These are all conditions that would otherwise be considered unfavorable for further strengthening and are often a consequence of the storm experiencing unfavorable winds in its environment. Storms with these characteristics can, however, strengthen and the goal of this experiment is to understand the physical processes and structures that govern whether storms will intensify in this type of environment.

Early Stage Science Objective(s) Addressed:

1. Collect datasets that can be used to improve the understanding of intensity change processes, as well as the initialization and evaluation of 3-D numerical models, particularly for TCs experiencing moderate vertical wind shear [*APHEX Goals 1, 3*].
2. Obtain a quantitative description of the kinematic and thermodynamic structure and evolution of intense convective systems (convective bursts) and the nearby environment to examine their role in TC intensity change [*APHEX Goals 1, 3*].
3. Improve our understanding of the physical processes responsible for the formation and evolution of arc clouds, as well as their impacts on TC structure and intensity in the short-term [*APHEX Goals 1, 3*].
4. Test new (or improved) technologies with the potential to fill gaps, both spatially and temporally, in the existing suite of airborne measurements in early stage TCs. These measurements include improved three-dimensional representation of the TC wind field, more spatially dense thermodynamic sampling of the boundary layer, and more accurate measurements of ocean surface winds [*APHEX Goal 2*]

EARLY STAGE EXPERIMENT
Science Description

Motivation: While some improvements in operational TC intensity forecasting have been made in recent years (DeMaria et al. 2014; Cangialosi et al. 2020), predicting changes in TC intensity (as defined by the 1-min. maximum sustained wind) remains problematic. In particular, the operational prediction of rapid intensification (RI) has proven to be especially difficult (Kaplan et al. 2010, Trabling and Bell 2020). The significant impact of such episodes has prompted the Tropical Prediction Center/National Hurricane Center (TPC/NHC) to declare it as its top forecast priority (Rappaport et al. 2009).

One specific challenge in forecasting TC intensity change is understanding how vertical wind shear (VWS) influences the storm (DeMaria and Kaplan 1994). While the response of storms to low magnitude VWS (favoring strengthening) and high VWS (favoring weakening) are well accepted, storm response in the moderate shear range (i.e., 4.5 to 11 m s⁻¹) can vary greatly (Bhatia and Nolan 2013). When VWS works together with dry environmental air, TC development is further limited (Tang and Emanuel 2012; Alland et al. 2021a, b; Fischer et al. 2023). However, the pathways by which VWS and dry air work together in nature to limit TC development remain unclear.

VWS is only one of many factors that affect processes that govern TC intensification, which span spatial and temporal scales from the environmental to vortex to convective and smaller scales. Other factors, including the radial and azimuthal distribution of latent heating in the inner core, vertical alignment of the vortex, environmental mid-tropospheric relative humidity (RH), static stability, boundary layer equivalent potential temperature, and sea surface temperature (SST) are also key to understanding RI. Understanding the communication of those impacts from the TC near-environment (~150–300 km from the TC center) to the inner core (within 150 km), how they vary across time scales, and their impact on inner-core RI processes is critical.

Background: Prior studies have found a number of large-scale environmental factors that are generally favorable for TC intensification, including low environmental vertical wind shear, high ocean heat content, and elevated low- to mid-tropospheric humidity. On the vortex scale, the rate of TC intensification in early-stage TCs — particularly those weaker storms, generally tropical storm strength or less, which are in the beginning stages of organization — have been shown to be related to the degree of symmetry of precipitation (Alvey et al. 2020; Chen et al. 2018a, 2021). Observational studies have also found that intensifying TCs typically have more symmetrically distributed precipitation and deep convection than non-intensifying TCs (e.g., Rogers et al. 2013, 2015, 2016; Alvey et al. 2015; Tao and Jiang 2015; Wadler et al. 2018a). The conclusions from these studies are consistent with idealized modeling studies that show that TC intensification is most sensitive to the axisymmetric, azimuthal wavenumber-0 component of diabatic heating (e.g., Nolan et al. 2007).

One principal environmental factor that can prevent the development of precipitation symmetry is VWS. The interaction of TCs with environmental VWS typically results in a wavenumber-1 asymmetry in vertical motion and precipitation, in which upward vertical motion and deep convection are favored in the downshear semicircle, while downward motion and suppression of deep convection is observed in the upshear semicircle (e.g., Marks et al. 1992; Reasor et al. 2000,

EARLY STAGE EXPERIMENT

Science Description

2013; Rogers et al. 2016; Zawislak et al. 2016). Subsidence in the upshear quadrants can increase the temperature and decrease the relative humidity of the middle troposphere, effectively capping (stabilizing) the lower troposphere (e.g., Nguyen et al. 2017). An increase in precipitation asymmetry can lead to the decrease in the projection of diabatic heating onto the axisymmetric, azimuthal wavenumber-0 component that has been shown to be important for TC intensification. However, the magnitude of this asymmetry can exhibit considerable variability, particularly within the moderate shear regime (4.5 to 11 m s⁻¹) that has been shown to be problematic for operational intensity forecasts (Bhatia and Nolan 2013).

This suggests the importance of identifying and understanding the environmental and internal (within the inner core) mechanisms that govern the azimuthal distribution of precipitation as well as its modes (i.e., shallow, moderately deep, and deep convection, and stratiform rain), thereby improving the understanding of the intensification process. Recent studies indicate that these mechanisms may include: the interaction of the vortex with environmental VWS and dry air, ventilation, vortex-scale subsidence, surface enthalpy fluxes from the underlying ocean, tropospheric stability, as well as the accompanying areally-averaged vertical mass flux profile.

VWS and dry air can work together to limit TC development via ventilation, defined as the flux of low-equivalent potential temperature (θ_E) environmental air into the TC inner core (Simpson and Riehl 1958; Cram et al. 2007; Riemer et al. 2010; Tang and Emanuel 2012; Munsell et al. 2013). Dry air can ventilate the subcloud layer via convective downdrafts (downdraft ventilation) (Riemer et al. 2010; Alland et al. 2021a). Dry air can also ventilate rising air in the eyewall via the inward radial transport (radial ventilation; Alland et al. 2021b). Didlake and Houze (2013) documented a potentially separate ventilation pathway in Hurricane Rita (2005), which had strong descending radial inflow associated with a stratiform rainband. This inflow was associated with low- θ_E air at middle and low levels, and may transport dry air into convection (e.g., radial ventilation) or downward into the subcloud layer (e.g., downdraft ventilation).

Overall, ventilation pathways can modulate the spatial structure of precipitation, especially upshear, which has been shown to be associated with TC intensity change (e.g., Rogers et al. 2013; Alvey et al. 2015; Tao and Jiang 2015; Rios-Berrios 2016a, b; Nguyen et al. 2017; Fischer et al. 2018, Rios-Berrios et al. 2018; Fischer et al. 2023). The majority of studies investigating the effects of ventilation on TC development have focused on mature TCs, but the effects for weak tropical cyclones have not received much attention. Recent work has used idealized modeling to document the effects of ventilation pathways on TC development for weak TCs (Alland et al. 2021a, b). These experiments showed the modulating effects on TC development to be:

1. Downdraft ventilation, which transported low- θ_E air left-of-shear and upshear between heights of 0 and 3 km associated with the principal rainband;
2. Radial ventilation, which transported low- θ_E air left-of-shear and upshear between heights of 0 and 3 km associated with the principal rainband (coupled with downdraft ventilation), and upshear and right-of-shear between heights of 5 and 9 km associated with a vertically-tilted TC vortex.

EARLY STAGE EXPERIMENT

Science Description

Both of these ventilation pathways aided in reducing the area of strong upward motions ($w > 0.5 \text{ m s}^{-1}$), reducing the vertical mass flux in the inner core, and limiting TC development. However, these experiments were simplified (e.g., linear wind profile with height, constant SST, dry air surrounding the TC). How do these ventilation pathways modulate TC development for a real storm? Observations are necessary to document the importance of these ventilation pathways, and their spatial structures, on precipitation symmetry and TC development so the atmospheric science community can verify models and better predict TC intensity change.

In addition to the ventilation pathways described above, air-sea fluxes can modulate boundary layer temperature and moisture and determine the likelihood that precipitation will become more symmetric. Under certain oceanic conditions the air-sea enthalpy fluxes can lead to recovery of low- θ_E air in the boundary layer (Tang and Emanuel 2012; Molinari et al. 2013; Zhang et al. 2013, 2017; Wadler et al. 2018b; Nguyen et al. 2019; Chen et al. 2021). In particular, Nguyen et al. (2019) showed that initially weak TCs that underwent intensification tend to have larger enthalpy fluxes in the upshear quadrants than weakening TCs; Chen et al. (2021) attributed the strong deep convection in the upshear quadrants of intensifying TCs to the boundary layer recovery of downdraft-cooled parcels originated from the downshear-left quadrant using a Lagrangian trajectory analysis. Observations are necessary to document the importance of the ventilation pathways and boundary layer recovery described here on precipitation symmetrization and TC development so the atmospheric science community can verify models and better predict TC intensity change.

Goal(s): Collect aircraft observations that will allow us to characterize the precipitation and vortex-scale kinematic and thermodynamic structures of TCs experiencing moderate vertical shear. Understanding the reasons behind these structures, particularly greater azimuthal coverage of precipitation and boundary layer ventilation and recovery, will contribute toward a greater understanding of the physical processes that govern whether TCs will intensify, (especially those that undergo RI) in this type of environment.

Hypotheses: The following hypotheses are guided by the theory that the thermodynamic and kinematic variability in the region of the TC near-environment (i.e., ~150–300 km from the TC center) are communicated to the inner core (<150 km from the center), which subsequently impacts the precipitation (i.e., latent heating) distribution in a way that may be favorable for TC (rapid) intensification.

Inner core Processes

1. The local kinematic (e.g., shear, vertical alignment of the vortex, inertial stability), thermodynamic (e.g., SST, static stability, and moisture/RH), and boundary layer properties (e.g., strength and depth of radial inflow, SST, surface enthalpy flux) are key in governing the precipitation modes and whether that precipitation is symmetrically distributed, which is a favorable configuration for intensification.

EARLY STAGE EXPERIMENT

Science Description

- a. The middle troposphere is moistened upshear due to detrainment from mid-tropospheric congestus, evaporation of falling stratiform rain, or reduced lateral advection of dry air from the environment
 - b. The lower troposphere is convectively unstable in the upshear quadrants due to enhanced surface enthalpy fluxes from the underlying ocean and/or reduced convective downdrafts
2. The presence of dry air and VWS alone does not guarantee that intensification will be limited; instead, the competition between VWS-induced ventilation and boundary layer recovery matters. Downdraft and/or radial ventilation must occur for the combined effects of dry air and VWS to limit TC development.
 - a. Downdraft ventilation influences TC development by transporting low- θ_E air downward left-of-shear and upshear (cyclonically downwind of convection). This low- θ_E air modulates convection left-of-shear and upshear.
 - b. Radial ventilation influences TC development by modulating convection in two ways:
 - i. At low levels, radial ventilation is coupled with downdraft ventilation and is associated with rainband activity.
 - ii. At middle and upper levels, radial ventilation, due to storm-relative flow associated with a tilted vortex and/or a weak vortex circulation, transports low- θ_E air upshear and right-of-shear. Convection occurring downshear is relatively protected from this dry air, unless the VWS magnitude is sufficiently strong.

Near-environment Processes:

1. Boundary layer inflow strength and depth in the near-environment varies diurnally with maxima (minima) in the early morning (afternoon) that represents a relatively favorable (unfavorable) period for intensification.
2. TC diurnal pulses exhibit squall-line-like behaviors as they propagate away from the TC each day and can initiate strong convectively-driven downdrafts in the near-environment, particularly in dry air positioned upshear, that temporarily disrupt the boundary layer via drying and enhanced static stability.

Objectives:

1. Quantify inner core and near-environment thermodynamic and kinematic variability, specifically as they relate to the precipitation modes and spatial distributions observed within the inner core during changes in TC intensity;
2. Observe diurnal variability in the TC planetary boundary layer, in particular changes to the radial inflow strength, and its relationship with the timing of intensity change;

EARLY STAGE EXPERIMENT

Science Description

3. Use observations within the inner core and near-environment to assess whether hypothesized downdraft and radial ventilation is occurring, and, if so, which specific pathways are affecting the inner convective structure and distribution; such as from the downward transport of low- θ_E air (downdraft ventilation), inward transport of low- θ_E air (radial ventilation), and the subsequent PBL recovery from surface enthalpy fluxes.

Overall, these objectives convey the need for a systematic, three-dimensional examination of physical processes near and within the TC inner core that act to modulate the spatial structure of convection, the thermodynamic and kinematic structures, and potentially, the intensity of a TC. Observations can also be compared with model and satellite-derived quantities (e.g., wind, moisture) to improve satellite algorithms and evaluate model representations (e.g., parameterizations, initial vortex structure) (APHEX Goal #1). TCs that are experiencing moderate vertical wind shear (4.5 to 11 m s⁻¹) over a deep layer (850–200 hPa) are of particular interest, since this range of shear values is often associated with considerable uncertainty with respect to the prospect for TC intensification (Bhatia and Nolan 2013).

Aircraft Pattern/Module Descriptions (see *Flight Pattern* document for more detailed information): Missions will be targeted for systems that have a reasonable chance of undergoing intensification based on statistical and numerical model forecast guidance. When possible (i.e., subject to range, timing, and other logistical constraints), missions will begin at least 24 h prior to the expected onset of intensification, while the TC is still at tropical depression or tropical storm intensity. This enables the documentation of TC structure during the time leading up to intensification onset (if it indeed occurs). Ideally missions will continue every 12 to 24 h (or more frequent, depending on the *Scenario* below), as long as feasible. Although all intensification rates are of interest, priority will be given to those with a high potential for RI according to model guidance and/or are forecast to experience at least moderate (4.5 to 11 m s⁻¹) vertical wind shear over a deep layer.

P-3 Pattern #1: A standard Figure-4 pattern centered on the estimated low-level or mid-level center, oriented such that the radial passes are aligned through approximately the upshear, downshear, left-of-shear, and right-of-shear directions, or alternatively along and perpendicular to the direction of vertical tilt of the circulation center. This pattern can also be flown oriented within the quadrants; i.e., 45° [downshear right], 315° [downshear left], 225° [upshear left], 135° [upshear right]) and rotated to complete a full rotated Figure-4 or flown with repeated azimuths to complete a repeated Figure-4. See the *Flight Pattern document* for how expendables are distributed.

P-3 Pattern #2: A standard Butterfly pattern centered on the estimated low-level or mid-level center. The butterfly should be oriented such that the upshear / uptilt semicircle (or downshear / downtilt if precipitation sampling is preferred in an asymmetric precipitation configuration) contains the most radial legs. See the *Flight Pattern document* for how expendables are distributed.

P-3 Module #1 (“Upshear Circumnavigation Module”): Sample the upshear semicircle, including the boundary between no convection and convection, if such a boundary exists, at up to three possible radii: 90 n mi (167 km), 60 n mi (111 km), and 40 n mi (74 km). Release up to 8

EARLY STAGE EXPERIMENT
Science Description

dropsondes per radius, as equally spaced as possible. The P-3 should operate as high as possible. This high-altitude circumnavigation allows for increased azimuthal and vertical dropsonde data coverage, particularly in the critical, precipitation-free upshear region that may fill in as intensification commences.

P-3 Module #2 (“Dry Air Entrainment Module”): Follow the dry air and precipitation free region (between eyewall / inner core convection and principal / outer rainbands), potentially radially inward, while flying downwind to the next pass and operating at the maximum allowable altitude. Dropsonde frequency should be increased (every 10 n mi) near the precipitation interface.

G-IV Pattern #1: A standard octagonal circumnavigation pattern centered on the estimated low-level or mid-level center. Radius of each circumnavigation is: 150 n mi (277 km), 90 n mi (167 km), 60 n mi (111 km). Dropsondes are released at each turn point, and in between turn points when a higher density is desired.

G-IV Pattern #2: A standard Star with Circumnavigation pattern. If desired, the outer points can be oriented to align with the VWS or vertical tilt vector. Supplemental observations can also be made when model sensitivity regions are indicated (e.g., derived from ECMWF and the COAMPS-TC model ensembles) that could positively impact forecasts of TC track, intensity and/or structure. Dropsondes are released at each turn point, and in between turn points when a higher density is desired.

G-IV Pattern #3: A standard Figure-4 with Double Circumnavigation pattern with radial legs in the Fig. 4 extending up to 150 n mi (275 km) and radii of 90 and 210 n mi (165 and 390 km) for the circumnavigations. If desired, the pattern can be centered on the estimated low-level or mid-level center, oriented such that the Fig. 4 radial passes are aligned through approximately the upshear, downshear, left-of-shear, and right-of-shear directions, or oriented relative to the vertical tilt of the circulation. If time is not available to complete the full pattern, the Fig. 4 is prioritized with either the inner or outer circumnavigation. Dropsonde are released at each turn point, midpoint, and center on each pass of the Fig. 4, and another at the midpoint of downwind leg; dropsondes also released at each turnpoint of the circumnavigations, with option to release in between each turnpoint to increase the density.

Scenario #1: One P-3 and the G-IV, simultaneous

One P-3 will fly Pattern #1 (Figure-4) or Pattern #2 (Butterfly) with the option to either follow the initial Figure-4 / butterfly with Module #1 (“Upshear Circumnavigation Module”, depending on the extent of the precipitation in the upshear semicircle that may pose limitations on flight altitudes above the freezing level), Module #2 (“Dry Air Entrainment”, depending on the extent of the precipitation that may pose limitations on flight altitudes above the freezing level), or rotate and complete a second Figure-4, or fly the same oriented Figure-4. After an initial Fig. 4 centered on the low-level center, the subsequent Fig. 4 could be centered on a mid-level center if it is able to be determined in real-time, likely by using the TDR analyses. If available, an sUAS can be released during either or both P-3 missions to complete an “Inflow Module” outlined in *RICO SUAVE*,

EARLY STAGE EXPERIMENT
Science Description

ideally being flown in the PBL below 1000 ft (305 m), and released left-of-shear, flown cyclonically to the downshear right quadrant, and subsequently penetrating the eyewall into the eye.

In this scenario, the G-IV will observe the outer to near-TC environment [~ 60 n mi (100 km) and outward to ~ 160 n mi (~ 300 km) from the center] using the circumnavigation in Pattern #1 or Pattern #2 (Star with Circumnavigation, which should be oriented with two outer points being upshear or uptilt), or Pattern #3 (Fig. 4 with Double Circumnavigation), if no P-3 has achieved higher-altitude dropsonde releases near the TC center. This scenario leaves the possibility open to 12-hourly (twice-a-day) coordinated missions.

Scenario #2: Only one P-3 available (no G-IV)

When the G-IV and 2nd P-3 is not available for coordinated operations, either because of operational tasking requirements or aircraft unavailability, P-3 targeted observations in the near environment and inner core can still contribute towards the objectives of the experiment. In this scenario there are two possible strategies for sampling, which depend on whether the precipitation distribution is asymmetric:

a. TC is highly asymmetric:

This option will be chosen when the precipitation distribution in the targeted TC is expected to be highly asymmetric during the mission. Such an asymmetric configuration would allow for a high-altitude P-3 upshear circumnavigation pattern (P-3 Module #1) to at least target the precipitation free upshear semicircle, and when hazard avoidance is possible, to extend the circumnavigation to the downshear quadrants.

Indications of an appropriate magnitude of asymmetry may include:

- 1) Visible, infrared, or microwave satellite imagery indicates an exposed or partially-exposed low-level circulation center (see example below).
- 2) The environmental vertical wind shear, as indicated by SHIPS, is expected to be sufficient ($> 4.5 \text{ m s}^{-1}$) during the mission to result in an asymmetric precipitation structure.
- 3) High-resolution numerical guidance (i.e. HAFS) forecast a lack of precipitation in the upshear semicircle of the TC during the mission.

EARLY STAGE EXPERIMENT
Science Description

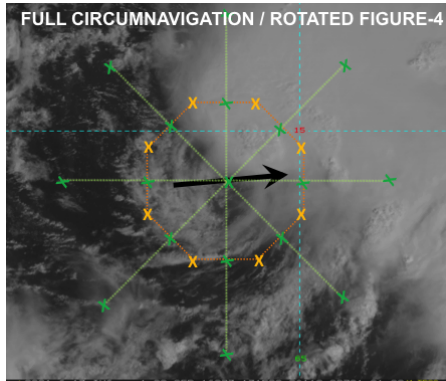


Figure-4 in green, circumnavigation in orange, shear vector in black, 'X' is a dropsonde location).

Given this scenario, the P-3 will sample the near environment and inner core with a pattern that includes a high-altitude circumnavigation and, optimally, a rotated Figure-4 in P-3 Pattern #1 or butterfly in P-3 Pattern #2. If time doesn't permit for a complete rotated Figure-4, then a single Figure-4 can be substituted.

b. TC is relatively symmetric:

This scenario applies to a targeted TC that has the potential for intensification, but the precipitation is expected to be too symmetric during the mission for the P-3 high-altitude circumnavigation to be conducted safely. Here, the P-3 will sample the inner-core vortex structure with a standard rotated Figure-4 (P-3 Pattern #1) or butterfly (P-3 Pattern #2) pattern.

Scenario #3: Only G-IV available (no P-3s)

This option is less preferable as targeted observations of the vortex structure are also important towards the objectives of the experiment. This option applies to any targeted TC that has the potential for intensification, regardless of asymmetric structure. Under this option, ideally the G-IV will sample the outer and near environment, and inner core with the Figure-4 with Double Circumnavigation (G-IV Pattern #3), but, if not, then minimally either the circumnavigation (G-IV Pattern #1) or star with circumnavigation (G-IV Pattern #2). Pattern #3 requires that hazard avoidance permit the G-IV to obtain measurements within/very near the inner core.

Links to Other Early Stage Experiments/Modules: If the opportunity arises during the execution of AIPEX, fly the *Vortex Alignment Module*, *Flight-Level Assessment of Intensification in Moderate Shear Module*, *Convective Burst Module*, or *Arc Cloud Module* (see accompanying discussion in Field Program plan). The *Vortex Alignment Module* is likely to be a key element of a coordinated experiment, since vortex misalignment is often an important driver of asymmetries in precipitation. The *Flight-Level Assessment of Intensification in Moderate Shear Module* will document the evolution of wind maxima at flight-level during the intensification process. The

EARLY STAGE EXPERIMENT
Science Description

Convective Burst Module would be optimal for determining the structure and evolution of deep convection within the framework of the broader vortex-scale circulation as it interacts with vertical shear (if appropriate) and local thermodynamic environment, while the *Arc Cloud Module* would be ideal for documenting locations within the vortex circulation encountering significant low- to mid-level dry air and determining the impact of the associated outflow boundaries on the boundary layer temperature and moisture distribution (an example of the communication that occurs between the inner core and near environment). AIPEX can also be flown in conjunction with the following Early Stage experiments and modules: *Surface Wind and Wave Validation Module*, *Stratiform Spiral Module*, *Ocean Survey Experiment* (in storm), *Sustained and Targeted Ocean Observations ITOFS*, *Evaluation of Tropical Cyclone Environment using Satellite Soundings Experiment*, *Hurricane Boundary Layer Module*, *Ventilation Module*, *Vortex Alignment Module*, or with *RICO SUAVE* in the Mature Stage.

Analysis Strategy: The general analysis strategy follows that performed in recent observational and modeling studies (e.g., Reasor et al. 2013; Zhang et al. 2013; Rogers et al. 2015; Rogers et al. 2016; Zawislak et al. 2016; Nguyen et al. 2017; Rios-Berrios et al. 2018, Nguyen et al. 2019, Rogers et al. 2020, Alland et al. 2020a, b; Wadler et al. 2021; Chen et al. 2018a, 2021). The analysis strategy includes assessing and documenting the time evolution of the following:

- *Vortex tilt* (P-3 TDR, possibly G-IV TDR). Assuming sufficient TDR coverage, the vortex tilt will be examined quantitatively by merging TDR analyses from each Figure-4 or by using individual radial passes, given sufficient coverage of scatterers. If the vortex tilt appears to decrease rapidly during a flight, individual TDR analyses can be used to examine the time evolution of vortex tilt during the alignment process by flying the *Vortex Alignment Module*.
- *Azimuthal and radial distribution of inner-core precipitation and deep convection* (P-3 TDR/LF, possibly G-IV TDR). The inner-core precipitation asymmetry, and its projection onto the axisymmetric, azimuthal wavenumber-0 component will be assessed quantitatively (assuming sufficient azimuthal coverage). The location of precipitation and convective bursts relative to the RMW will be examined.
- *Precipitation mode* (P-3 TDR/LF, possibly G-IV TDR). An analysis of the precipitation mode (shallow, moderately deep, deep convection, as well as stratiform rain), using the vertical velocity and reflectivity structure, will allow for an assessment as to whether moistening of the inner core occurs through upscale growth of convection (moistening from convective detrainment at gradually higher altitudes), or from the top-down via stratiform rain as hydrometeors produced downshear are transported azimuthally upshear.
- *Low-wavenumber thermodynamic and kinematic structure of the boundary layer* (P-3/GIV dropsondes, DWL for kinematic only), including surface fluxes of heat, moisture, and momentum. The thermodynamic focus will be on the boundary layer cooling by convective downdrafts and the subsequent recovery via surface enthalpy fluxes from the underlying ocean in the downstream (upshear-left through downshear-right) quadrants. Surface enthalpy fluxes will be calculated where dropsondes are paired with AXBTs that provide SST, and/or from sUAS and IRsonde measurements. The kinematic focus will be on

EARLY STAGE EXPERIMENT
Science Description

obtaining measurements of the strength and depth of boundary layer inflow and convergence in the boundary layer, both in a symmetric sense and relative to the shear vector (when relevant). Additionally, the gradient and agradient flow in the boundary layer will be calculated.

- *Low-wavenumber thermodynamic and kinematic structure above the boundary layer* (P-3/G-IV dropsondes, P-3/G-IV TDR and DWL for kinematic only). The presence of mid-tropospheric dry air is of particular interest. Assuming mid-tropospheric dry air is present (most likely in the upshear quadrants), the potential sources of this dry air (vortex-scale subsidence or lateral advection from the environment) and how this upshear dry air is removed (i.e., through detrainment from congestus or evaporation of stratiform precipitation) will be assessed.
- *Vertical wind shear and upper-level divergence* (G-IV dropsondes). These quantities will be computed and compared with global model analyses. The vertical distribution of shear will also be evaluated (i.e., VWS calculations in different vertical levels outside of the standard 850 to 200 hPa will be calculated, c.f. Finocchio et al. 2016, 2017), as upper-level shear is hypothesized to be less deleterious than low-level shear.
- *Ventilation* will be quantified by combining the thermodynamic data from dropsondes with wind analyses from dropsondes and the TDR. Radial and downdraft ventilation will both be calculated. It will be important to obtain deep vertical profiles of thermodynamic and kinematic data in the left-of-shear and upshear semicircles to determine the vertical extent of ventilation pathways. The necessity for thermodynamic and kinematic coverage left-of-shear and upshear is why it is recommended to release more dropsondes than the standard flight patterns/modules.

The overarching hypothesis is that by performing the above analyses for multiple AIPEX data sets collected during both RI and non-RI events it will be possible to determine the conditions that are triggers for RI. This analysis strategy can also assist in the evaluation of 3-D numerical models, including the sufficiency (or lack thereof) of the horizontal resolution, and the microphysical and planetary boundary layer parameterization schemes. Dropsonde, flight-level, super-obbed Doppler radar, and SFMR data are made available over the GTS and assimilated in real time, while full Doppler fields and lower fuselage radar will be available post-flight.

References:

- Alland, J. J., B. H. Tang, K. L. Corbosiero, and G. H. Bryan, 2021a: Combined effects of midlevel dry air and vertical wind shear on tropical cyclone development. Part I: Downdraft ventilation. *J. Atmos. Sci.*, **78(3)**, 763–782, doi: <https://doi.org/10.1175/JAS-D-20-0054.1>.
- Alland, J. J., B. H. Tang, K. L. Corbosiero, and G. H. Bryan, 2021b: Combined effects of midlevel dry air and vertical wind shear on tropical cyclone development. Part II: Radial ventilation. *J. Atmos. Sci.*, **78(3)**, 783–796, <https://doi.org/10.1175/JAS-D-20-0055.1>.

EARLY STAGE EXPERIMENT

Science Description

Alvey III, G. R., J. Zawislak, and E. Zipser, 2015: Precipitation Properties Observed during Tropical Cyclone Intensity Change. *Mon. Wea. Rev.*, **143**, 4476–4492. doi: 10.1175/MWR-D-15-0065.1.

Alvey, G. R., III, E. Zipser, and J. Zawislak, 2020: How does Hurricane Edouard (2014) evolve toward symmetry before rapid intensification? A high-resolution ensemble study. *J. Atmos. Sci.*, **77**, 1329–1351, <https://doi.org/10.1175/JAS-D-18-0355.1>.

Alvey, G. R., III, M. Fischer, P. Reasor, J. Zawislak, and R. Rogers, 2022: Observed Processes Underlying the Favorable Vortex Repositioning Early in the Development of Hurricane Dorian (2019). *Mon. Wea. Rev.*, **150**, 193–213, doi:10.1175/MWR-D-21-0069.1.

Bhatia, K. T., and D. S. Nolan, 2013: Relating the skill of tropical cyclone intensity forecasts to the synoptic environment. *Wea. Forecasting*, **28**, 961–980, doi: 10.1175/WAF-D-12-00110.1.

Cangialosi, J. P., E. Blake, M. DeMaria, A. Penny, A. Latta, and E. Rappaport, 2020: Recent Progress in Tropical Cyclone Intensity Forecasting at the National Hurricane Center. *Wea. Forecasting*, **35**, 1913–1922, doi:10.1175/WAF-D-20-0059.1.

Chen, X., M. Xue, and J. Fang, 2018a: Rapid intensification of Typhoon Mujigae (2015) under different sea surface temperatures: Structural changes leading to rapid intensification. *J. Atmos. Sci.*, **75**, 4313–4335, doi:10.1175/JAS-D-18-0017.1.

Chen, X., Y. Wang, J. Fang, and M. Xue, 2018b: A Numerical Study on Rapid Intensification of Typhoon Vicente (2012) in the South China Sea. Part II: Roles of Inner-core Processes. *J. Atmos. Sci.*, **75**, 235–255, doi:10.1175/JAS-D-17-0129.1.

Chen, X., J. A. Zhang, and F. D. Marks, 2019: A Thermodynamic Pathway Leading to Rapid Intensification of Tropical Cyclones in Shear. *Geo. Res. Lett.*, **46**, 9241–9251.

Chen, X., J.-F. Gu, J. A. Zhang, F. D. Marks, R. F. Rogers, and J. J. Cione, 2021: Boundary layer recovery and precipitation symmetrization preceding rapid intensification of tropical cyclones under shear. *J. Atmos. Sci.*, **78**, 1523–1544, doi:10.1175/JAS-D-20-0252.1.

Cram, T. A., J. Persing, M. T. Montgomery, and S. A. Braun, 2007: A Lagrangian trajectory view on transport and mixing processes between the eye, eyewall, and environment using a high-resolution simulation of Hurricane Bonnie (1998). *J. Atmos. Sci.*, **64**, 1835–1856, doi:10.1175/JAS3921.1.

DeMaria, M., and J. Kaplan, 1994: A statistical hurricane intensity prediction scheme (SHIPS) for the Atlantic basin. *Wea. Forecasting*, **9**, 209–220, doi:10.1175/1520-0434(1994)0092.0.CO;2.

DeMaria, M., M. Mainelli, L. K. Shay, J. A. Knaff, and J. Kaplan, 2005: Further improvements to the statistical hurricane intensity prediction scheme (SHIPS). *Wea. Forecasting*, **20**, 531–543, doi:10.1175/WAF862.1.

EARLY STAGE EXPERIMENT

Science Description

DeMaria, M., C. R. Sampson, J. A. Knaff, and K. D. Musgrave, 2014: Is tropical cyclone intensity guidance improving? *Bull. Amer. Meteor. Soc.*, **95**, 387–398, doi:10.1175/BAMS-D-12-00240.1.

Didlake, A. C., and R. A. Houze, 2013: Dynamics of the stratiform sector of a tropical cyclone rainband. *J. Atmos. Sci.*, **70**, 1891–1911, doi:10.1175/JAS-D-12-0245.1.

Finocchio, P. M., S. J. Majumdar, D. S. Nolan, and M. Iskandarani, 2016: Idealized tropical cyclone responses to the height and depth of environmental vertical wind shear. *Mon. Wea. Rev.*, **144**, 2155–2175, doi:10.1175/MWR-D-15-0320.1.

Finocchio, P. M., and S. J. Majumdar, 2017: A statistical perspective on wind profiles and vertical wind shear in tropical cyclone environments of the Northern Hemisphere. *Mon. Wea. Rev.*, **145**, 361–378, doi:10.1175/MWR-D-16-0221.1.

Fischer, M. S., P. D., Reasor, R. F. Rogers, and J. F. Gamache, 2022: An analysis of tropical cyclone vortex and convective characteristics in relation to storm intensity using a novel airborne Doppler radar database. *Mon. Wea. Rev.*, **150**, 2255–2278.

Fischer, M. S., P. D. Reasor, B. H. Tang, K. L. Corbosiero, R. D. Torn, and X. Chen, 2023: A tale of two vortex evolutions: Using a high-resolution ensemble to assess the impacts of ventilation on a tropical cyclone rapid intensification event. *Mon. Wea. Rev.*, **151**, 297–320.

Gjorgjievska, S., and D. J. Raymond, 2014: Interaction between dynamics and thermodynamics during tropical cyclogenesis. *Atmos. Chem. and Phys.*, **14**, 3065–3082, doi:10.5194/784 acp-14-3065-2014.

Kaplan, J., M. DeMaria, and J. A. Knaff, 2010: A revised tropical cyclone rapid intensification index for the Atlantic and eastern North Pacific basins. *Wea. Forecasting*, **25**, 220–241, doi: 10.1175/2009WAF2222280.1.

Kaplan, J., and Coauthors, 2015: Evaluating environmental impacts on tropical cyclone rapid intensification predictability utilizing statistical models. *Wea. Forecasting*, **30**, 1374–1396, doi: 10.1175/WAF-D-15-0032.1.

Marks, F. D., Jr., R. A. Houze Jr., and J. F. Gamache, 1992: Dual-aircraft investigation of the inner core of Hurricane Norbert. Part I: Kinematic structure. *J. Atmos. Sci.*, **49**, 919–942, doi: 10.1175/1520-0469(1992)049<0919:DAIOTI>2.0.CO;2.

Molinari, J., J. Frank, and D. Vollaro, 2013: Convective Bursts, Downdraft Cooling, and Boundary Layer Recovery in a Sheared Tropical Storm. *Mon. Wea. Rev.*, **141**, 1048–1060, doi: 10.1175/MWR-D-12-00135.1.

Munsell, E. B., F. Zhang, and D. P. Stern, 2013: Predictability and dynamics of a nonintensifying tropical storm: Erika (2009). *J. Atmos. Sci.*, **70**, 2505–2524, doi:10.1175/JAS-D-12-0243.1.

Nguyen, L. T., R. Rogers, and P. Reasor 2017: Thermodynamic and kinematic influences on precipitation symmetry in sheared tropical cyclones: Bertha and Cristobal (2014). *Mon.*

EARLY STAGE EXPERIMENT
Science Description

Wea. Rev., **145**, 4423–4446, <https://doi.org/10.1175/MWR-D-17-0073.1>

Nguyen, L.T., R. Rogers, J. Zawislak, and J.A. Zhang, 2019: Assessing the Influence of Convective Downdrafts and Surface Enthalpy Fluxes on Tropical Cyclone Intensity Change in Moderate Vertical Wind Shear. *Mon. Wea. Rev.*, **147**, 3519–3534, <https://doi.org/10.1175/MWR-D-18-0461.1>

Nolan, D. S., Y. Moon, and D. P. Stern, 2007: Tropical cyclone intensification from asymmetric convection: Energetics and efficiency. *J. Atmos. Sci.*, **64**, 3377–3405, doi: 10.1175/JAS3988.1.

Rappaport, E. N., and Coauthors, 2009: Advances and Challenges at the National Hurricane Center. *Wea. Forecasting*, **24**, 395–419.

Raymond, D. J., S. L. Sessions, and C. L. Carrillo, 2011: Thermodynamics of tropical cyclogenesis in the northwest pacific. *J. Geophys. Res. Atmos.*, **116** (D18), doi:10.1029/2011JD015624

Reasor, P. D., M. T. Montgomery, F. D. Marks, and J. F. Gamache, 2000: Low-wavenumber structure and evolution of the hurricane inner core observed by airborne dual-Doppler radar. *Mon. Wea. Rev.*, **128**, 1653–1680, doi:10.1175/1520-0493(2000)1282.0.CO;2.

Reasor, P. D., R. F. Rogers, and S. Lorsolo, 2013: Environmental flow impacts on tropical cyclone structure diagnosed from airborne Doppler radar composites. *Mon. Wea. Rev.*, **141**, 2949–2969, doi: 10.1175/MWR-D-12-00334.1.

Riemer, M., M. T. Montgomery, and M. E. Nicholls, 2010: A new paradigm for intensity modification of tropical cyclones: Thermodynamic impact of vertical wind shear on the inflow layer. *Atmos. Chem. Phys.*, **10**, 3163–3188, doi:10.5194/acp-10-3163-2010.

Rios-Berrios, R., R. D. Torn, and C. A. Davis, 2016a: An ensemble approach to investigate tropical cyclone intensification in sheared environments. Part I: Katia (2011). *J. Atmos. Sci.*, **73**, 71–93, doi:10.1175/jas-d-15-0052.1.

Rios-Berrios, R., R. D. Torn, and C. A. Davis, 2016b: An ensemble approach to investigate tropical cyclone intensification in sheared environments. Part II: Ophelia (2011). *J. Atmos. Sci.*, **73**, 1555–1575, doi:10.1175/jas-d-15-0245.1.

Rios-Berrios, R., C. A. Davis, and R. D. Torn, 2018: A hypothesis for the intensification of tropical cyclones under moderate vertical wind shear. *J. Atmos. Sci.*, **75**, 4149–4173, doi:10.1175/jas-d-18-0070.1.

Rios-Berrios, R., 2020: Impacts of Radiation and Cold Pools on the Intensity and Vortex Tilt of Weak Tropical Cyclones Interacting with Vertical Wind Shear. *J. Atmos. Sci.*, **77**, 669–689, doi:10.1175/JAS-D-19-0159.1.

Rogers, R., P. Reasor, and S. Lorsolo, 2013: Airborne Doppler observations of the inner-core structural differences between intensifying and steady-state tropical cyclones. *Mon. Wea. Rev.*, **141**, 2970–2991, doi: 10.1175/MWR-D-12-00357.1.

EARLY STAGE EXPERIMENT
Science Description

- Rogers, R. F., P. D. Reasor, and J. A. Zhang, 2015: Multiscale structure and evolution of Hurricane Earl (2010) during rapid intensification. *Mon. Wea. Rev.*, **143**, 536–562, doi: 10.1175/MWR-D-14-00175.1.
- Rogers, R., J. Zhang, J. Zawislak, H. Jiang, G. Alvey, E. Zipser, and S. Stevenson, 2016: Observations of the structure and evolution of Hurricane Edouard (2014) during intensity change. Part II: Kinematic structure and the distribution of deep convection. *Mon. Wea. Rev.*, **144**, 3355–3376, doi: 10.1175/MWR-D-16-0017.1.
- Rogers, R. F., P. D. Reasor, J. A. Zawislak, and L. T. Nguyen, 2020: Precipitation Processes and Vortex Alignment during the Intensification of a Weak Tropical Cyclone in Moderate Vertical Shear. *Mon. Wea. Rev.*, **148**, 1899–1929, <https://doi.org/10.1175/MWR-D-19-0315.1>
- Rozoff, C. M., and J. P. Kossin, 2011: New probabilistic forecast models for the prediction of tropical cyclone rapid intensification. *Wea. Forecasting*, **26**, 677–689, doi: 10.1175/WAF-D-10-05059.1.
- Schechter, D. A., and K. Menelaou, 2020: Development of a Misaligned Tropical Cyclone. *J. Atmos. Sci.*, **77**, 79–111, doi:10.1175/JAS-D-19-0074.1.
- Schechter, D. A., 2022: Intensification of Tilted Tropical Cyclones over Relatively Cool and Warm Oceans in Idealized Numerical Simulations. *J. Atmos. Sci.*, **79**, 485–512, doi:10.1175/JAS-D-21-0051.1
- Schubert, W. H., and J. J. Hack, 1982: Inertial stability and tropical cyclone development. *J. Atmos. Sci.*, **39**, 1687–1697, doi:10.1175/1520-0469(1982)039<1687:ISATCD>2.0.CO;2.
- Simpson, R., and R. Riehl, 1958: Mid-tropospheric ventilation as a constraint on hurricane development and maintenance. Tech. Conf. on Hurricanes, Amer. Meteor. Soc., Miami Beach, FL, D4–1–D4–10.
- Smith, R.K. and Montgomery, M.T. (2016), The efficiency of diabatic heating and tropical cyclone intensification. *Q.J.R. Meteorol. Soc.*, **142**, 2081–2086, doi:10.1002/qj.2804
- Sumwalt, R. L., C. A. Hart, E. F. Weener, and T. B. Dinh-Zahr, 2017: Tropical cyclone information for mariners. National Transportation Safety Board safety recommendation report, 21 pp, <https://www.nts.gov/investigations/AccidentReports/Reports/MSR1702.pdf>.
- Tang, B., and K. Emanuel, 2012: Sensitivity of tropical cyclone intensity to ventilation in an axisymmetric model. *J. Atmos. Sci.*, **69**, 2394–2413, doi:10.1175/jas-d-11-0232.1.
- Tao, C., and H. Jiang, 2015: Distributions of shallow to very deep precipitation–convection in rapidly intensifying tropical cyclones. *J. Climate*, **28**, 8791–8824, doi: 10.1175/JCLI-D-14-00448.1.

EARLY STAGE EXPERIMENT

Science Description

Trabing, B. C., and M. M. Bell, 2020: Understanding Error Distributions of Hurricane Intensity Forecasts during Rapid Intensity Changes. *Wea. Forecasting*, **35**, 2219–2234, <https://doi.org/10.1175/WAF-D-19-0253.1>.

Vigh, J. L., and W. H. Schubert, 2009: Rapid development of the tropical cyclone warm core. *J. Atmos. Sci.*, **66**, 3335–3350, doi: 10.1175/2009JAS3092.1.

Wadler, J.B., R.F. Rogers, and P.D. Reasor, 2018a: The Relationship Between Spatial Variations in the Structure of Convective Bursts and Tropical Cyclone Intensification as Determined by Airborne Doppler Radar. *Mon. Wea. Rev.*, **146**, 761–780, <https://doi.org/10.1175/MWR-D-17-0213.1>

Wadler, J.B., J.A. Zhang, B. Jaimes, and L.K. Shay, 2018b: Dwndrafts and the Evolution of Boundary Layer Thermodynamics in Hurricane Earl (2010) before and during Rapid Intensification. *Mon. Wea. Rev.*, **146**, 3545–3565, <https://doi.org/10.1175/MWR-D-18-0090.1>

Wadler, J.B., J.A. Zhang, R.F. Rogers, B. Jaimes, and L.K. Shay, 2021: The Rapid Intensification of Hurricane Michael (2018): Storm Structure and the Relationship to Environmental and Air-Sea Interactions; *Mon. Wea. Rev.*, **149**, 245-267, <https://doi.org/10.1175/MWR-D-20-0145.1>

Zawislak, J., H. Jiang, G. Alvey, E. Zipser, R. Rogers, J. Zhang, and S. Stevenson, 2016: Observations of the structure and evolution of Hurricane Edouard (2014) during intensity change. Part I: Relationship between the thermodynamic structure and precipitation. *Mon. Wea. Rev.*, **144**, 3333–3354, doi: 10.1175/MWR-D-16-0017.1.

Zhang, J. A., R. F. Rogers, P. Reasor, E. Uhlhorn, and F. D. Marks Jr., 2013: Asymmetric hurricane boundary layer structure from dropsonde composites in relation to the environmental wind shear. *Mon. Wea. Rev.*, **141**, 3968–3984, doi: 10.1175/MWR-D-12-00335.1.

Zhang, J.A., J. J. Cione, E. A. Kalina, E.W. Uhlhorn, T. Hock, and J.A. Smith, 2017: Observations of infrared sea surface temperature and air-sea interaction in Hurricane Edouard (2014) using GPS dropsondes. *J. Atmos. Oceanic Technol.*, **0**, doi: 10.1175/JTECH-D-16-0211.1.